

# Delving into Inter-Image Invariance for Unsupervised Visual Representations

Jiahao Xie<sup>1</sup> Xiaohang Zhan<sup>2</sup> Ziwei Liu<sup>1</sup> Yew Soon Ong<sup>1</sup> Chen Change Loy<sup>1</sup>

<sup>1</sup>Nanyang Technological University <sup>2</sup>The Chinese University of Hong Kong

{jiahao003, ziwei.liu, asysong, ccloy}@ntu.edu.sg xiaohangzhan@outlook.com

## Abstract

Contrastive learning has recently shown immense potential in unsupervised visual representation learning. Existing studies in this track mainly focus on intra-image invariance learning. The learning typically uses rich intra-image transformations to construct positive pairs and then maximizes agreement using a contrastive loss. The merits of inter-image invariance, conversely, remain much less explored. One major obstacle to exploit inter-image invariance is that it is unclear how to reliably construct inter-image positive pairs, and further derive effective supervision from them since there are no pair annotations available. In this work, we present a rigorous and comprehensive study on inter-image invariance learning from three main constituting components: pseudo-label maintenance, sampling strategy, and decision boundary design. Through carefully-designed comparisons and analysis, we propose a unified and generic framework that supports the integration of unsupervised intra- and inter-image invariance learning. With all the obtained recipes, our final model, namely *InterCLR*, shows consistent improvements over state-of-the-art intra-image invariance learning methods on multiple standard benchmarks. Codes will be released at <https://github.com/open-mmlab/OpenSelfSup>.

## 1. Introduction

Unsupervised representation learning witnesses substantial progress thanks to the emergence of self-supervised learning, which can be broadly divided into four categories: recovery-based [14, 30, 41, 43, 54, 57], transformation prediction [16, 19, 36, 56], clustering-based [1, 4–6, 28, 50, 51, 55], and contrastive learning [8, 22, 23, 27, 39, 42, 45, 49, 52, 60]. Among the various paradigms, contrastive learning shows great potential and even surpasses supervised learning [8, 22, 23]. A typical contrastive learning method applies rich transformations to an image and maximizes agreement between the original image and the transformed ones, or between the images in two transformations via a contrastive loss in the latent feature space. This process encourages the network to learn “intra-image” invariance (*i.e.*, instance

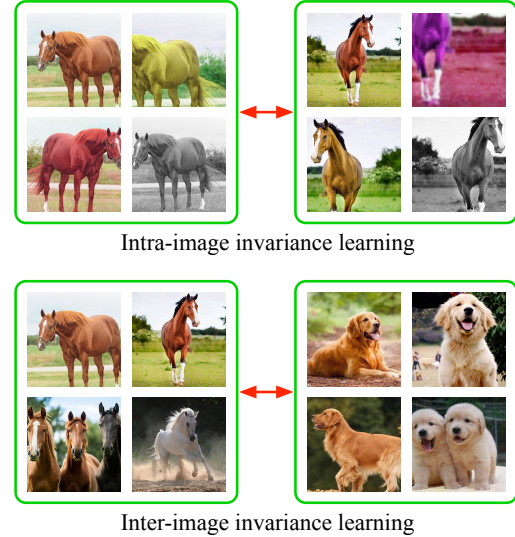


Figure 1. Intra-image invariance learning groups different augmented views of the same image together while separates different images apart. In contrast, inter-image invariance learning groups similar images together while separates dissimilar ones apart.

discrimination [49]).

Some typical “intra-image” transformations, including random cropping, resizing, flipping and color distortion, are shown in Figure 1. Clearly, it is challenging to design convincing transformations to faithfully cover all the natural variances existing in natural images. Hence, it remains an open question whether the existing form of transformations can sufficiently lead to our ideal representations, which should be invariant to viewpoints, occlusions, poses, instance-level or subclass-level differences. Such variances naturally exist between pairs of instances belonging to the same semantic class. However, it is challenging to exploit such “inter-image” invariance in the context of unsupervised learning since no pair annotations are available. Clustering is a plausible solution to derive such pseudo-labels for contrastive learning. For instance, LA [60] adopted off-the-shelf clustering to obtain pseudo-labels to constitute “inter-image” candidates. Nevertheless, the performance still falls behind state-of-the-art intra-image based methods. We believe there exist details that might have been over-

looked, if resolved, shall make the usefulness of inter-image invariance learning more pronounced than it currently does.

In this work, we carefully investigate the usefulness of inter-image invariance from three major aspects:

**1) Pseudo-label maintenance.** Owing to expensive computational cost, global clustering adopted in DeepCluster [4] and LA [60] can only be performed sparsely every several training epochs. Hence, it inevitably produces stale labels relative to the rapidly updated network. To re-assign pseudo-labels continuously and instantly, we consider mini-batch  $k$ -means in place of global  $k$ -means by integrating the label and centroid update steps into each training iteration. In this way, clustering and network update are simultaneously undertaken, yielding more reliable pseudo-labels.

**2) Sampling strategy.** It is common for supervised learning to adopt hard negative mining. However, in the scenario of unsupervised learning, hard negatives might well have wrong labels, *i.e.*, they may be actually positive pairs. However, if we choose easy negative pairs and push them apart, they will still be easy negatives next time, and might never be corrected, leading to a shortcut solution. Hence, the sampling strategy in unsupervised inter-image invariance learning is non-trivial, which has so far been neglected.

**3) Decision boundary design.** Existing works [13, 34, 35, 46, 47] in supervised learning design large-margin loss functions to learn discriminative features. While in unsupervised learning, it is unsure whether pursuing discriminative features benefits since pseudo-labels are noisy. For example, if a positive pair of images are misclassified as a negative one, the large-margin optimization strategy will further push them apart. Then the situation will never be corrected. We explore decision margin designs for both the unsupervised intra- and inter-image branches.

**Contributions** – This study reveals key aspects that should be carefully considered when leveraging inter-image information in unsupervised contrastive learning. Although some of these aspects were originally considered in supervised learning, the conclusions are quite different and unique in the unsupervised scenario. To the best of our knowledge, this is the first empirical study on the effects of these aspects for unsupervised contrastive representations. The merits of inter-image invariance learning are revealed through its consistent improvements over state-of-the-art intra-image invariance learning methods on standard unsupervised representation learning benchmarks.

## 2. Related work

**Contrastive-based representation learning.** Contrastive-based methods learn invariant features by contrasting positive samples against negative ones. A positive pair is usually formed with two augmented views of the same image, while negative ones are formed with different images. Typically, the positive and negative samples can be obtained

either within a batch or from a memory bank. In batch-wise methods [2, 8, 26, 27, 42, 52], positive and negative samples are drawn from the current mini-batch with the same encoder that is updated end-to-end with back-propagation. For methods based on memory bank [39, 45, 49, 60], positive and negative samples are drawn from a memory bank that stores features of all samples computed in previous steps. Recently, He *et al.* [23] propose MoCo to build large and consistent dictionaries for contrastive learning using a slowly progressing encoder. Grill *et al.* [22] further propose BYOL to learn invariant features without negative samples. As opposed to our work, the aforementioned approaches only explore intra-image statistics for contrastive learning. Although LA [60] is the first attempt to leverage inter-image statistics for contrastive learning, it mainly focuses on designing sampling metric while leaving other important aspects unexplored. We show that pseudo-label maintenance, sampling strategy and decision boundary design have to be collectively considered for good results.

**Clustering-based representation learning.** Earlier attempts have shown great potential of joint clustering and feature learning, but the studies are limited to small datasets [3, 7, 29, 32, 50, 51]. DeepCluster [4] (DC) scales up the learning to millions of images through alternating between deep feature clustering and CNN parameters update. Although DC uses clustering during representation learning, it differs from our work conceptually in two aspects. First, DC optimizes the cross-entropy loss between predictions and pseudo-labels obtained by cluster assignments. Such optimization requires an additional parametric classifier. Second, DC adopts offline global clustering that unavoidably permutes label assignments randomly in different epochs. As a result, the classifier has to be frequently reinitialized after each label reassignment, which leads to training instability. In contrast, we optimize a non-parametric classifier at instance level and integrate the label update procedure into each training iteration with online clustering. ODC [55] also performs online clustering. Our work differs to theirs in that ODC follows DC to optimize the cross-entropy loss between predicted and cluster labels, requiring the computationally expensive parametric classifier. In addition, ODC uses loss re-weighting to handle clustering distribution, while InterCLR directly uses online mini-batch  $k$ -means without resorting to other specific techniques. Experiments in Section 5 show that InterCLR substantially outperforms ODC. Recently, Caron *et al.* [6] propose SwAV to enforce consistent cluster-assignment prediction between multiple views of the same image. The cluster assignments are produced by the Sinkhorn-Knopp transform [11] under an equipartition constraint similar in [1]. As opposed to our work, SwAV compare cluster assignments of the same instance, whereas we sample and compare different instances with the cluster assignments.

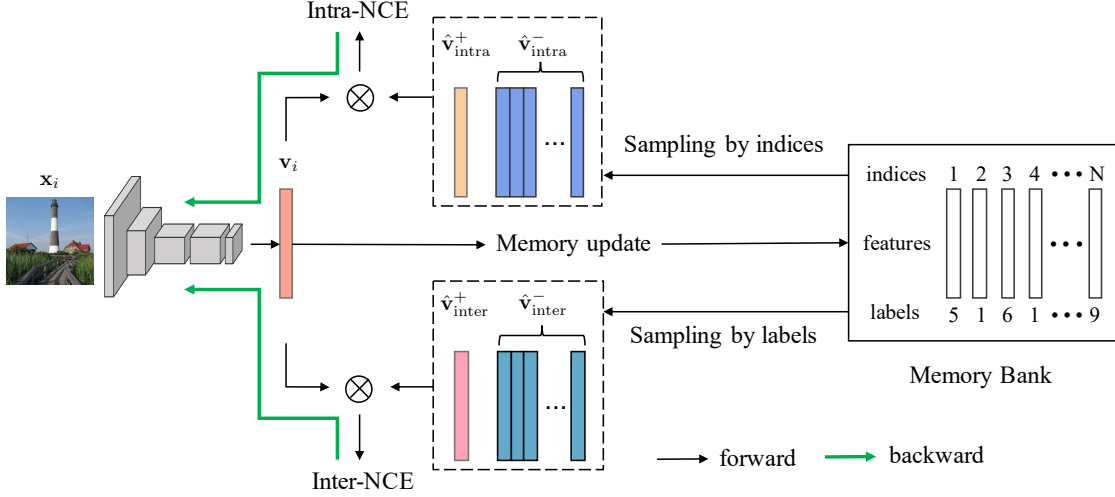


Figure 2. Overview of our unified intra- and inter-image invariance learning framework (InterCLR). For the intra-image component, positive and negative pairs are sampled by indices, while for the inter-image part, they are sampled by pseudo-labels. The memory bank including features and pseudo-labels is updated in each iteration. “Intra-NCE” and “Inter-NCE” constitute loss functions for the two branches, respectively.

### 3. Preliminaries

**Intra-image invariance learning.** A contrastive representation learning method typically learns a neural encoder  $f_\theta(\cdot)$  that maps training images  $\mathbf{I} = \{x_1, x_2, \dots, x_N\}$  to compact features  $\mathbf{V} = \{v_1, v_2, \dots, v_N\}$  with  $v_i = f_\theta(x_i)$  in a  $D$ -dimensional L2-normalized embedding space, where the samples of a positive pair are pulled together and those of negative pairs are pushed apart. For intra-image invariance learning, the positive pair is usually formed with two different augmented views of the same image while the negative pairs are obtained from different images. To achieve this objective, a contrastive loss function is optimized with similarity measured by dot product. Here we consider an effective form of contrastive loss function, called InfoNCE [42], as follows:

$$\mathcal{L}_{\text{InfoNCE}} = \sum_{i=1}^N -\log \frac{\exp(v_i \cdot v_i^+ / \tau)}{\exp(v_i \cdot v_i^+ / \tau) + \sum_{v_i^- \in \mathbf{V}_K} \exp(v_i \cdot v_i^- / \tau)}, \quad (1)$$

where  $\tau$  is a temperature hyper-parameter,  $v_i^+$  is a positive sample for instance  $i$ , and  $v_i^- \in \mathbf{V}_K \subseteq \mathbf{V} \setminus \{v_i\}$  denotes a set of  $K$  negative samples randomly drawn from the training images excluding instance  $i$ .

**Memory bank.** Contrastive learning requires a large number of negative samples to learn good representations [42, 49]. However, the number of negatives is usually limited by the mini-batch size. While simply increasing the batch to a large size (e.g., 4k-8k) can achieve good performance [8], it requires huge computational resources. To address this issue, one can use a memory bank to store running average features of all samples in the dataset computed in previous steps. Formally, let  $\hat{\mathbf{V}} = \{\hat{v}_1, \hat{v}_2, \dots, \hat{v}_N\}$  denote the stored

features in the memory bank, these features are updated by:

$$\hat{v}_i \leftarrow (1 - \omega) \hat{v}_i + \omega v_i, \quad (2)$$

where  $\omega \in (0, 1]$  is a momentum coefficient. With a set of features  $\hat{\mathbf{V}}$ , we can then replace  $\mathbf{V}$  with  $\hat{\mathbf{V}}$  in Equation (1) without having to recompute all the features every time.

### 4. Methodology

Based on the aforementioned intra-image invariance learning, we describe how to extend the notion to leverage inter-image statistics for contrastive learning.

As shown in Figure 2, we introduce two invariance learning branches in our framework, one for intra-image and the other for inter-image. The intra-image branch draws contrastive pairs by indices following the conventional protocol. The inter-image counterpart constructs contrastive pairs with pseudo-labels obtained by clustering: a positive sample for an input image is selected within the same cluster while the negative samples are obtained from other clusters. We use variants of InfoNCE described in Section 3 as our contrastive loss and perform back-propagation to update the networks. Within the inter-image branch, three components have non-trivial effects on learned representations and require specific designs, i.e., 1) pseudo-label maintenance, 2) sampling strategy for contrastive pairs, and 3) decision boundary design for the loss function.

#### 4.1. Maintaining pseudo-labels

To avoid stale labels from offline clustering, we adopt mini-batch  $k$ -means to integrate label update into the network update iterations, thus updating the pseudo-labels on-the-fly. Formally, we first initialize all the features, labels

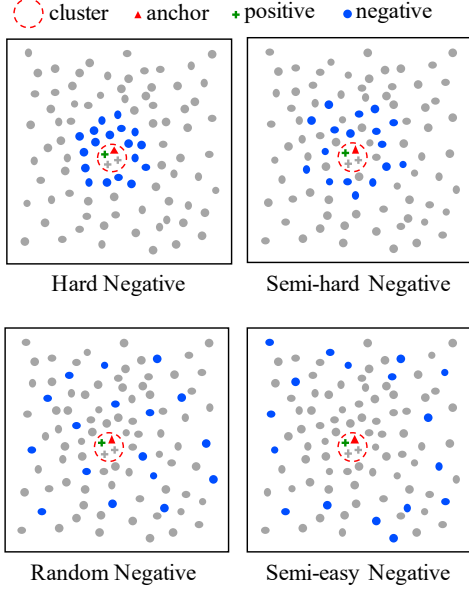


Figure 3. Different negative sampling strategies in the embedding space. Given an anchor (red triangle), the positive sample candidates (crosses) are those points within the cluster represented by the dashed red circle while the negative sample candidates (dots) are the points beyond this cluster. The positive sample (green cross) is drawn randomly from the cluster while the negative samples (blue dots) are drawn with different sampling strategies.

and centroids via a global clustering process, *e.g.*,  $k$ -means. Next, in a mini-batch stochastic gradient descent iteration, the forward batch features are used to update the corresponding stored features in the memory bank with Equation (2). Meanwhile, the label of each involved sample is updated by finding its current nearest centroid following  $\min_{\mathbf{y}_i \in \{0,1\}^k, \text{ s.t. } \mathbf{y}_i^T \mathbf{1} = 1} \|\hat{\mathbf{v}}_i - \mathbf{C}\mathbf{y}_i\|_2^2$ , where  $k$  is the number of clusters,  $\mathbf{C} \in \mathbb{R}^{d \times k}$  is a recorded centroid matrix with each column representing a temporary cluster centroid that evolves during training,  $\mathbf{y}_i$  is a  $k$ -dimensional one-hot vector indicating the label assignment for instance  $i$ . Finally, the recorded centroid matrix is updated by averaging all the features belonging to their current and respective clusters. In this way, labels are updated instantly along with the features.

## 4.2. Sampling contrastive pairs

As discussed in Section 1, sampling positive and negative pairs in unsupervised inter-image invariance learning is non-trivial. To investigate the effect of sampling, we design and compare four sampling strategies for negative samples: *hard*, *semi-hard*, *random*, and *semi-easy*.

We define samples sharing the same label with the input image  $\mathbf{x}_i$  in the memory bank as positive sample candidates  $\mathcal{S}_i^p$ , while others as negative sample candidates  $\mathcal{S}_i^n$ . For positive sampling, we randomly draw one sample from  $\mathcal{S}_i^p$  and use it to form a positive pair with  $\mathbf{v}_i$ . For negative sampling,

we sample  $K$  negatives from  $\mathcal{S}_i^n$ .

As shown in a schematic illustration in Figure 3, for “hard negative” sampling, we sample  $K$  nearest neighbors of  $\mathbf{v}_i$  from  $\mathcal{S}_i^n$  using cosine distance criterion. For “semi-hard negative” sampling, we first create a relatively larger nearest neighbor pool, *i.e.*, top 10% nearest neighbors from  $\mathcal{S}_i^n$ , then we randomly draw  $K$  samples from this pool. For “random negative” sampling, we simply draw  $K$  negative samples at random from  $\mathcal{S}_i^n$ . For “semi-easy negative” sampling, similar to the “semi-hard negative” strategy, we first sample a pool with top 10% farthest neighbors from  $\mathcal{S}_i^n$ , then we randomly draw  $K$  samples from this pool. We do not include an “easy negative” strategy that chooses the top  $K$  easiest negatives. As mentioned in Section 1, the easiest samples are prone to a shortcut solution.

## 4.3. Designing decision boundary

Designing decision boundary for unsupervised inter-image invariance learning needs special care as pseudo-labels are noisy. Here, we present a way that allows decision margins to be more stringent or looser to suit the variability required in our task.

Considering the contrastive loss in Equation (1), since features in the embedding space are L2-normalized, we replace  $\mathbf{v}_i \cdot \mathbf{v}_j$  with  $\cos(\theta_{\mathbf{v}_i, \mathbf{v}_j})$ . For simplicity of analysis, we consider the case where there is only one negative sample, *i.e.*, a binary classification scenario. The contrastive loss thus results in a zero-margin decision boundary given by:

$$\cos(\theta_{\mathbf{v}_i, \mathbf{v}_i^+}) = \cos(\theta_{\mathbf{v}_i, \mathbf{v}_i^-}). \quad (3)$$

To allow the decision margins to be more stringent or looser, we first introduce a cosine decision margin  $m$  such that the decision boundary becomes:

$$\begin{aligned} C_+ : \cos(\theta_{\mathbf{v}_i, \mathbf{v}_i^+}) - m &\geq \cos(\theta_{\mathbf{v}_i, \mathbf{v}_i^-}), \\ C_- : \cos(\theta_{\mathbf{v}_i, \mathbf{v}_i^-}) - m &\geq \cos(\theta_{\mathbf{v}_i, \mathbf{v}_i^+}). \end{aligned} \quad (4)$$

As shown in Figure 4,  $m > 0$  indicates a more stringent decision boundary that encourages the discriminative ability of the representations, while  $m < 0$  stands for a looser decision boundary. Then, we define a margin contrastive loss (MarginNCE) as:

$$\mathcal{L}_{\text{MarginNCE}} = \sum_{i=1}^N -\log \frac{\exp\left(\left(\cos(\theta_{\mathbf{v}_i, \mathbf{v}_i^+}) - m\right)/\tau\right)}{\exp\left(\left(\cos(\theta_{\mathbf{v}_i, \mathbf{v}_i^+}) - m\right)/\tau\right) + \sum_{\mathbf{v}_i^- \in \mathcal{V}_K} \exp\left(\cos(\theta_{\mathbf{v}_i, \mathbf{v}_i^-})/\tau\right)}. \quad (5)$$

We make a hypothesis that for the intra-image MarginNCE loss ( $\mathcal{L}_{\text{Intra-MarginNCE}}$ ), the margin should be positive, since the labels derived from image indices are always correct; while for the inter-image MarginNCE loss ( $\mathcal{L}_{\text{Inter-MarginNCE}}$ ), the margin should be negative, since the pseudo-labels are evolving during training and are not accurate enough. The



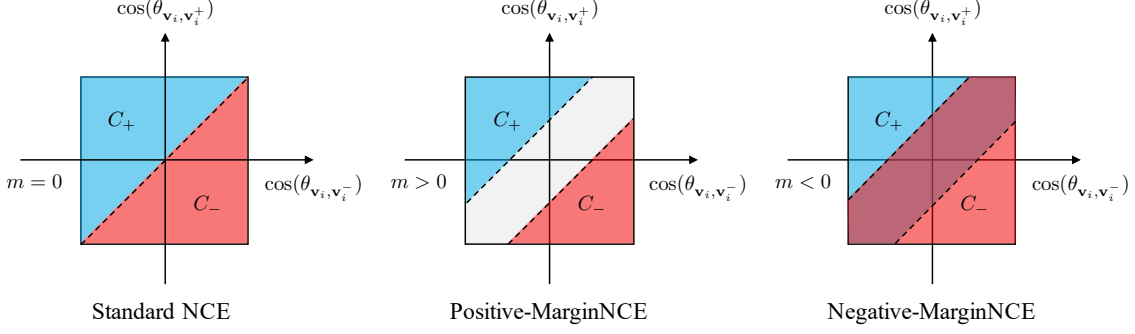


Figure 4. Comparison of different decision margins between standard NCE and MarginNCE under one negative sample case. The dashed line represents the decision boundary and the gray area (shown as wine red when  $C_+$  and  $C_-$  overlap) shows the decision margins.

final loss consists of these two MarginNCE loss functions:

$$\mathcal{L}_{\text{Intra-Inter-MarginNCE}} = \lambda \mathcal{L}_{\text{Intra-MarginNCE}} + (1 - \lambda) \mathcal{L}_{\text{Inter-MarginNCE}}, \quad (6)$$

where  $\lambda$  is the weight to balance the two terms. We study the effects of both  $m$  and  $\lambda$  in Section 5.3.

## 5. Experiments

### 5.1. Implementation details

**Baselines.** Our most essential intra-image invariance learning baseline is NPID [49]: it is the special case of InterCLR by setting  $\lambda = 1$  in Equation (6). We find it is possible to further improve the implementation of NPID by adopting more advanced techniques in [8]: a non-linear projection head (a 2-layer MLP) and stronger Gaussian blur augmentation. We denote our improved version of NPID as NPIDv2. Comparing InterCLR with NPIDv2 is critical to study the effect of inter-image invariance learning that InterCLR aims to achieve. In addition, to demonstrate that InterCLR is more generally applicable, we also experiment with most recent baselines, *i.e.*, MoCov2 [9] and BYOL [22].

**Training details.** We use ResNet-50 [25] as the default backbone and perform unsupervised pre-training on ImageNet [12] training set that contains 1.28M images without labels. Prior works [6, 8, 22, 26, 39] have shown that using a larger batch size or training for longer epochs can improve the performance of unsupervised representations. However, they usually come at the cost of huge computational resources. To ensure fair and direct comparisons, we generally follow *the same setting* of each baseline we experiment with and target at a more accessible training resource for InterCLR, *i.e.*, using a batch size of 256 for 200 epochs. We provide a full overview of all experimental settings in the appendix.

### 5.2. Results on standard benchmarks

Following common practice in self-supervised learning [20, 58], we evaluate the quality of learned representations by transferring to several standard downstream tasks.

**Image classification with linear models.** Following [20, 39], we freeze all the backbone parameters and train classifiers on representations from different depths of the network on three datasets, including ImageNet [12], Places205 [59] and VOC07 [17]. For ImageNet and Places205, we train a 1000-way and 205-way fully-connected classifier, respectively. For VOC07, we train linear SVMs following the same setting from [20, 39]. Table 1 shows the results for the best-performing layer of each method. Our improved NPIDv2 baseline already performs well on the three datasets. However, InterCLR substantially outperforms NPIDv2, demonstrating the benefits of introducing inter-image invariance. Similar improvements are observed in MoCov2 and BYOL. By building upon a stronger baseline in intra-image invariance learning, InterCLR outperforms previous self-supervised learners that are pre-trained within 200 epochs using a feasible 256 batch size on a standard ResNet-50 backbone, setting a new state of the art in this fair competition on all three datasets.

**Low-shot image classification.** Next, we explore the quality of learned representations when there are few training examples per category by transferring to the low-shot VOC07 classification task. Specifically, we vary the number of labeled examples in each class and train linear SVMs on the frozen backbone following the same setup in [20]. We report mAP across five independent samples for each low-shot value evaluated on the test split of VOC07. Table 1 shows the final mAP results of different methods obtained with the averages of all low-shot values and all independent runs. The per-shot results are given in the appendix. InterCLR substantially outperforms its intra-image invariance learning counterpart.

**Semi-supervised learning.** We perform semi-supervised learning experiments on ImageNet following the experimental setup of [39, 49]. We randomly select 1% and 10% subsets of the labeled ImageNet training data in a class-balanced way. Then, we fine-tune our models on these two subsets. We report top-5 accuracy on the official ImageNet validation split as shown in Table 2. Again, InterCLR boosts the performance of all tested intra-image invariance

Table 1. Image classification evaluation. We report top-1 center-crop accuracy of fully-connected classifiers for ImageNet and Places205, and mAP of linear SVMs for VOC07 and VOC07<sub>lowshot</sub>. We show the parameter counts of the feature extractors. Numbers with \* are from officially released pre-trained model. We re-implement 200-epoch SimCLR with a batch size of 256. SimCLR, NPIDv2, MoCo(v2) and InterCLR are pre-trained under the same batch size and epochs. For BYOL experiments, we use a batch size of 256 and accumulate gradients to simulate a batch size of 4096. All other numbers are taken from the papers as cited. Methods in the last section require either longer training epochs or larger architectures. <sup>†</sup>: SimCLR, BYOL and SwAV requires a large batch size of 4096 allocated on 128/512 GPUs/TPUs to obtain the optimal performance. AMDIM uses FastAutoAugment [33] that is supervised by ImageNet labels. <sup>‡</sup>: SwAV uses multi-crop augmentation giving additional 2-4% performance improvements. Results for SwAV without multi-crop augmentation are adopted from [10].

Method	Arch.	#Params (M)	#Epochs	Transfer Dataset			
				ImageNet	Places205	VOC07	VOC07 <sub>lowshot</sub>
Supervised [20]	R50	24	-	75.5	52.5	88.0	75.4
Random [20]	R50	24	-	13.7	16.6	9.6	9.0
<i>Methods using ResNet-50 within 200 training epochs:</i>							
Colorization [20]	R50	24	28	39.6	37.5	55.6	33.3
Jigsaw [20]	R50	24	90	45.7	41.2	64.5	39.2
NPID [49]	R50	24	200	54.0	45.5	-	-
Rotation [39]	R50	24	-	48.9	41.4	63.9	-
BigBiGAN [15]	R50	24	-	56.6	-	-	-
LA [60]	R50	24	200	58.8	49.1	-	-
MoCo [23]	R50	24	200	60.6	50.2*	79.3*	57.9*
SimCLR [8]	R50	24	200	61.9	51.6	79.0	58.4
SwAV [10]	R50	24	200	69.1	-	-	-
SimSiam [10]	R50	24	200	70.0	-	-	-
NPIDv2	R50	24	200	64.6	51.9	81.7	63.2
NPIDv2-InterCLR	R50	24	200	65.7	52.4	82.8	65.8
MoCov2 [9]	R50	24	200	67.5	52.5*	84.2*	68.2*
MoCov2-InterCLR	R50	24	200	68.0	52.6	84.9	<b>70.7</b>
BYOL [22]	R50	24	200	70.6	52.7	85.1	68.9
BYOL-InterCLR	R50	24	200	<b>72.6</b>	<b>53.7</b>	<b>86.6</b>	69.6
<i>Methods using other architectures or longer training epochs:</i>							
SeLa [1]	R50	24	400	61.5	-	-	-
ODC [55]	R50	24	440	57.6	49.3	78.2	57.1
PIRL [39]	R50	24	800	63.6	49.8	81.1	-
SimCLR [8]	R50	24	1000	69.3 <sup>†</sup>	-	-	-
BYOL [22]	R50	24	1000	74.3 <sup>†</sup>	-	-	-
SwAV [10]	R50	24	800	71.8 <sup>†</sup>	-	-	-
SwAV [6]	R50	24	800	75.3 <sup>‡</sup>	56.7 <sup>‡</sup>	88.9 <sup>‡</sup>	-
CPC [42]	R101	28	-	48.7	-	-	-
CPC v2 [26]	R170 <sub>wider</sub>	303	~200	65.9	-	-	-
CMC [45]	R50 <sub>L+ab</sub>	47	280	64.1	-	-	-
AMDIM [2]	Custom	626	150	68.1 <sup>†</sup>	55.0 <sup>†</sup>	-	-

learners by clear margins, especially when only 1% labeled data is available. We also observe that BYOL-InterCLR trained for only 200 epochs can achieve comparable results as BYOL trained for 1000 epochs. The result of 1% labeled data even surpasses SwAV trained for 800 epochs, achieving new state-of-the-art performance in this learning setting.

**Object detection.** Following [23], we use Detectron2 [48] to train the Faster-RCNN [44] object detection model with a R50-C4 backbone [24], with BatchNorm tuned. We fine-tune all layers on the trainval split of VOC07+12, and eval-

uate on the test split of VOC07. We use the same setup for both supervised and self-supervised models. As shown in Table 3, InterCLR outperforms both its intra-image invariance learning and supervised pre-training counterparts within 200 pre-training epochs.

### 5.3. Study and analysis

We give an in-depth analysis of our design for inter-image invariance learning in this subsection. To perform a large amount of experiments needed for the analysis, we ad-

Table 2. Semi-supervised learning on ImageNet. We report top-5 center-crop accuracy on the ImageNet validation set of self-supervised models that are fine-tuned with 1% and 10% of the labeled ImageNet training data. We use released pre-trained model for MoCo(v2), and re-implement SimCLR and BYOL. All other numbers are taken from the corresponding papers.

Method	Backbone	#Epochs	Label fraction	
			1%	10%
			Top-5 accuracy	
Supervised [53]	R50	-	48.4	80.4
Random [49]	R50	-	22.0	59.0
<i>Methods using semi-supervised learning:</i>				
Pseudo-label [31]	R50v2	-	51.6	82.4
VAT + Ent Min. [21,40]	R50v2	-	47.0	83.4
S <sup>4</sup> L Exemplar [53]	R50v2	-	47.0	83.7
S <sup>4</sup> L Rotation [53]	R50v2	-	53.4	83.8
<i>Methods using self-supervised learning only:</i>				
NPID [49]	R50	200	39.2	77.4
Jigsaw [20]	R50	90	45.3	79.3
MoCo [23]	R50	200	61.3	84.0
SimCLR [8]	R50	200	64.5	82.6
NPIDv2	R50	200	63.0	84.0
NPIDv2-InterCLR	R50	200	65.8	84.5
MoCov2 [9]	R50	200	67.7	85.1
MoCov2-InterCLR	R50	200	71.3	85.6
BYOL [22]	R50	200	76.8	87.8
BYOL-InterCLR	R50	200	<b>79.2</b>	<b>89.1</b>
PIRL [39]	R50	800	57.2	83.8
SimCLR [8]	R50	1000	75.5	87.8
BYOL [22]	R50	1000	78.4	89.0
SwAV [6]	R50	800	78.5	89.9

Table 3. Object detection fine-tuned on VOC07+12 using Faster-RCNN. We report AP<sub>50</sub>, the default metric for VOC object detection. All methods are pre-trained for 200 epochs on ImageNet for fair comparisons. Most numbers are directly taken from [10, 23].

Method	Architecture	#Epochs	VOC07+12
Random [23]	R50-C4	-	60.2
Supervised [23]	R50-C4	90	81.3
MoCo [23]	R50-C4	200	81.5
SimCLR [10]	R50-C4	200	81.8
SwAV [10]	R50-C4	200	81.5
SimSiam [10]	R50-C4	200	82.4
NPIDv2	R50-C4	200	81.5
NPIDv2-InterCLR	R50-C4	200	81.9
MoCov2 [9]	R50-C4	200	82.4
MoCov2-InterCLR	R50-C4	200	<b>82.6</b>
BYOL [10]	R50-C4	200	81.4
BYOL-InterCLR	R50-C4	200	82.3

just the experimental setting to train each model with fewer negative samples or for fewer epochs. Specifically, when

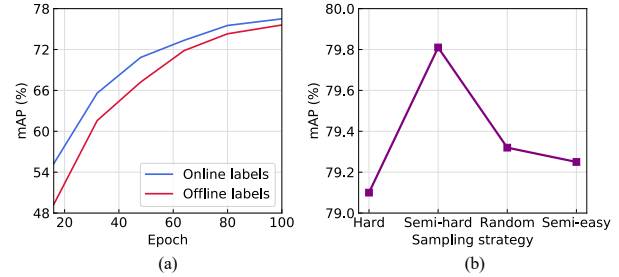


Figure 5. (a) Comparison between online labels and offline labels. (b) Comparison of different sampling strategies. We report mAP of linear SVMs on the VOC07 classification benchmark.

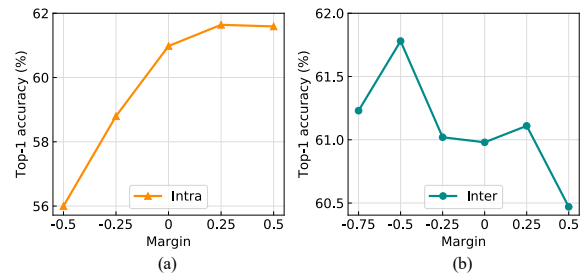


Figure 6. Effect of decision margin for (a) intra-image branch, and (b) inter-image branch. We report top-1 accuracy on the ImageNet linear classification benchmark.

studying the three main aspects, we train with 4096 negative samples for 100 epochs and perform a set of experiments progressively. For pseudo-label maintenance study, we use random negative sampling and zero-margin decision boundary. For sampling strategy study, we use online pseudo-label maintenance and zero-margin decision boundary. For decision boundary study, we use online pseudo-label maintenance and semi-hard negative sampling. When conducting the ablation on  $\lambda$  in Equation (6), we train with 4096 negative samples for 200 epochs. Besides, we use online pseudo-label maintenance, random negative sampling and zero-margin decision boundary. We keep the other hyper-parameters in Section 5.1 unchanged. As a result, we obtain relatively lower performances. However, these experiments aim at better understanding the properties of InterCLR and provide a useful guidance on how to design each component for inter-image invariance learning. Throughout the section, we take NPIDv2-InterCLR as the prototype for empirical study and use the standard benchmarks from Section 5.2 to measure the quality of learned representations.

**Online labels are better than offline labels.** We compare the effect of two investigated pseudo-label maintenance mechanisms (*i.e.*, online mini-batch  $k$ -means and offline global  $k$ -means) on learned representations. Figure 5(a) shows the results using these two mechanisms. We observe better performance and faster convergence of online labels over offline labels during the training process, suggesting the superiority of maintaining pseudo-labels online.

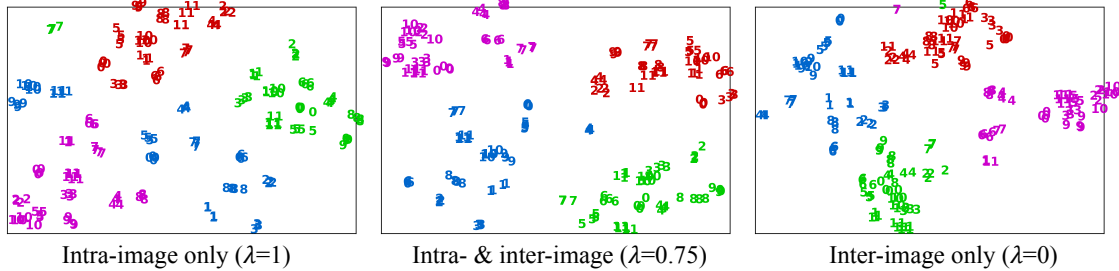


Figure 7. Feature space visualization. The features are embedded via t-SNE. The color indicates ImageNet original classes, and the number indicates different images in each class. Points with the same color and number are the same image in different augmentations.

**Semi-hard negative sampling wins out.** We then study the importance of negative sampling strategies. Figure 5(b) shows the comparison of four negative sampling strategies proposed in Section 4.2. Interestingly, we find that semi-hard negative sampling achieves the best performance, while hard negative sampling is even worse than the naïve random sampling strategy. The observation reveals that different from what is commonly adopted in supervised learning, hard negative mining is not the best choice in the unsupervised learning scenario. On the contrary, randomly sampled negatives within a relatively larger nearest neighbor pool are more reliable and unbiased for unsupervised inter-image invariance learning.

**Decision margins: positive for “Intra” and negative for “Inter”.** We study the impact of decision boundary using different cosine margins for the proposed MarginNCE loss. Specifically, we perform a set of margin experiments for each branch by setting the margin of the other branch as 0. Figure 6 shows the effect of different decision margins. For the intra-image branch shown in Figure 6(a), using a positive margin improves the performance upon zero-margin decision boundary, while a negative one degrades the performance. Hence, it is necessary to pursue discriminative features for intra-image invariance learning, which is in accordance with the situation of supervised learning. However, the opposite phenomenon is observed for the inter-image branch as shown in Figure 6(b). Using a negative margin (the best performance is observed when  $m = -0.5$ ) improves upon zero-margin decision boundary, while a positive one fluctuates and even degrades the performance. Therefore, rather than solely pursue discriminative features, it is beneficial to design a less stringent decision boundary for inter-image invariance learning.

**Analysis on intra- and inter-image invariance.** The benefits of inter-image invariance brought by InterCLR have been fully demonstrated on various downstream tasks in Section 5.2. Here, we analyze the effect of  $\lambda$  that controls the weight between two MarginNCE losses in Equation (6). For  $\lambda = 1$ , our framework degenerates to a typical form of intra-image invariance learning in [49]. For  $\lambda = 0$ , only the inter-image invariance learning branch is retained.

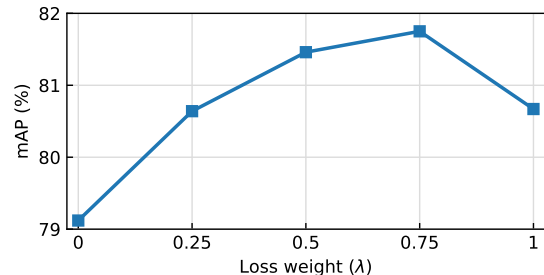


Figure 8. Effect of the trade-off hyper-parameter  $\lambda$  in Equation (6) on the quality of learned representations. We report mAP of linear SVMs on the VOC07 classification benchmark.

Figure 8 shows the effect of  $\lambda$  on the quality of InterCLR representations using the VOC07 classification benchmark. InterCLR benefits from the combination of two kinds of image invariance learning, with the best performance obtained by setting  $\lambda = 0.75$ . Furthermore, we also visualize the learned representations in the t-SNE [38] embedding space. As shown in Figure 7, the “Intra-image only” model merely groups the same image in different augmentations together; however, different images are separated even though in the same class. The “Inter-image only” model shortens the distance between images in the same class; however, outliers emerge. The “Intra- & inter-image” method well inherits the advantages from above two methods, resulting in a more separable feature space.

## 6. Conclusion

In this work, we have investigated into inter-image invariance learning from different perspectives and show the effect of different design choices, w.r.t. pseudo-label maintenance, sampling strategy, and decision boundary design. By combining our observations, we proposed a unified and generic framework, InterCLR, for unsupervised intra- and inter-image invariance learning. With this framework, we improve over previous intra-image invariance learning methods on multiple standard benchmarks under a fair setting. Our results demonstrate the potential of inter-image invariance learning to improve contrastive learning for unsupervised visual representations.



## References

- [1] Yuki Markus Asano, Christian Rupprecht, and Andrea Vedaldi. Self-labelling via simultaneous clustering and representation learning. In *ICLR*, 2020. 1, 2, 6
- [2] Philip Bachman, R Devon Hjelm, and William Buchwalter. Learning representations by maximizing mutual information across views. In *NeurIPS*, pages 15509–15519, 2019. 2, 6
- [3] Piotr Bojanowski and Armand Joulin. Unsupervised learning by predicting noise. In *ICML*, pages 517–526, 2017. 2
- [4] Mathilde Caron, Piotr Bojanowski, Armand Joulin, and Matthijs Douze. Deep clustering for unsupervised learning of visual features. In *ECCV*, 2018. 1, 2
- [5] Mathilde Caron, Piotr Bojanowski, Julien Mairal, and Armand Joulin. Unsupervised pre-training of image features on non-curated data. In *ICCV*, pages 2959–2968, 2019. 1
- [6] Mathilde Caron, Ishan Misra, Julien Mairal, Priya Goyal, Piotr Bojanowski, and Armand Joulin. Unsupervised learning of visual features by contrasting cluster assignments. *arXiv preprint arXiv:2006.09882*, 2020. 1, 2, 5, 6, 7
- [7] Jianlong Chang, Lingfeng Wang, Gaofeng Meng, Shiming Xiang, and Chunhong Pan. Deep adaptive image clustering. In *ICCV*, pages 5879–5887, 2017. 2
- [8] Ting Chen, Simon Kornblith, Mohammad Norouzi, and Geoffrey Hinton. A simple framework for contrastive learning of visual representations. *arXiv preprint arXiv:2002.05709*, 2020. 1, 2, 3, 5, 6, 7, 11
- [9] Xinlei Chen, Haoqi Fan, Ross Girshick, and Kaiming He. Improved baselines with momentum contrastive learning. *arXiv preprint arXiv:2003.04297*, 2020. 5, 6, 7, 11
- [10] Xinlei Chen and Kaiming He. Exploring simple siamese representation learning. *arXiv preprint arXiv:2011.10566*, 2020. 6, 7, 11, 12
- [11] Marco Cuturi. Sinkhorn distances: lightspeed computation of optimal transport. In *NeurIPS*, 2013. 2
- [12] Jia Deng, Wei Dong, Richard Socher, Li-Jia Li, Kai Li, and Li Fei-Fei. Imagenet: A large-scale hierarchical image database. In *CVPR*, pages 248–255, 2009. 5
- [13] Jiankang Deng, Jia Guo, Niannan Xue, and Stefanos Zafeiriou. Arcface: Additive angular margin loss for deep face recognition. In *CVPR*, pages 4690–4699, 2019. 2
- [14] Carl Doersch, Abhinav Gupta, and Alexei A Efros. Unsupervised visual representation learning by context prediction. In *ICCV*, 2015. 1
- [15] Jeff Donahue and Karen Simonyan. Large scale adversarial representation learning. In *NeurIPS*, pages 10541–10551, 2019. 6
- [16] Alexey Dosovitskiy, Jost Tobias Springenberg, Martin Riedmiller, and Thomas Brox. Discriminative unsupervised feature learning with convolutional neural networks. In *NeurIPS*, pages 766–774, 2014. 1
- [17] Mark Everingham, Luc Van Gool, Christopher KI Williams, John Winn, and Andrew Zisserman. The pascal visual object classes (voc) challenge. *IJCV*, 88(2):303–338, 2010. 5
- [18] Rong-En Fan, Kai-Wei Chang, Cho-Jui Hsieh, Xiang-Rui Wang, and Chih-Jen Lin. Liblinear: A library for large linear classification. *JMLR*, 9:1871–1874, 2008. 11
- [19] Spyros Gidaris, Praveer Singh, and Nikos Komodakis. Unsupervised representation learning by predicting image rotations. In *ICLR*, 2018. 1
- [20] Priya Goyal, Dhruv Mahajan, Abhinav Gupta, and Ishan Misra. Scaling and benchmarking self-supervised visual representation learning. In *ICCV*, pages 6391–6400, 2019. 5, 6, 7, 11
- [21] Yves Grandvalet and Yoshua Bengio. Semi-supervised learning by entropy minimization. In *NeurIPS*, pages 529–536, 2005. 7
- [22] Jean-Bastien Grill, Florian Strub, Florent Altché, Corentin Tallec, Pierre H Richemond, Elena Buchatskaya, Carl Doersch, Bernardo Avila Pires, Zhaohan Daniel Guo, Mohammad Gheshlaghi Azar, et al. Bootstrap your own latent: A new approach to self-supervised learning. *arXiv preprint arXiv:2006.07733*, 2020. 1, 2, 5, 6, 7, 11
- [23] Kaiming He, Haoqi Fan, Yuxin Wu, Saining Xie, and Ross Girshick. Momentum contrast for unsupervised visual representation learning. In *CVPR*, pages 9729–9738, 2020. 1, 2, 6, 7, 12
- [24] Kaiming He, Georgia Gkioxari, Piotr Dollár, and Ross Girshick. Mask r-cnn. In *ICCV*, pages 2961–2969, 2017. 6
- [25] Kaiming He, Xiangyu Zhang, Shaoqing Ren, and Jian Sun. Deep residual learning for image recognition. In *CVPR*, 2016. 5
- [26] Olivier J Hénaff, Aravind Srinivas, Jeffrey De Fauw, Ali Razavi, Carl Doersch, SM Eslami, and Aaron van den Oord. Data-efficient image recognition with contrastive predictive coding. *arXiv preprint arXiv:1905.09272*, 2019. 2, 5, 6
- [27] R Devon Hjelm, Alex Fedorov, Samuel Lavoie-Marchildon, Karan Grewal, Phil Bachman, Adam Trischler, and Yoshua Bengio. Learning deep representations by mutual information estimation and maximization. In *ICLR*, 2019. 1, 2
- [28] Chen Huang, Chen Change Loy, and Xiaoou Tang. Unsupervised learning of discriminative attributes and visual representations. In *CVPR*, 2016. 1
- [29] Xu Ji, João F Henriques, and Andrea Vedaldi. Invariant information clustering for unsupervised image classification and segmentation. In *ICCV*, pages 9865–9874, 2019. 2
- [30] Gustav Larsson, Michael Maire, and Gregory Shakhnarovich. Learning representations for automatic colorization. In *ECCV*, pages 577–593, 2016. 1
- [31] Dong-Hyun Lee. Pseudo-label: The simple and efficient semi-supervised learning method for deep neural networks. In *Workshop on challenges in representation learning, ICML*, volume 3, page 2, 2013. 7
- [32] Renjie Liao, Alex Schwing, Richard Zemel, and Raquel Urtasun. Learning deep parsimonious representations. In *NeurIPS*, pages 5076–5084, 2016. 2
- [33] Sungbin Lim, Ildoo Kim, Taesup Kim, Chiheon Kim, and Sungwoong Kim. Fast autoaugment. In *NeurIPS*, pages 6662–6672, 2019. 6
- [34] Weiyang Liu, Yandong Wen, Zhiding Yu, Ming Li, Bhiksha Raj, and Le Song. Sphreface: Deep hypersphere embedding for face recognition. In *CVPR*, pages 212–220, 2017. 2
- [35] Weiyang Liu, Yandong Wen, Zhiding Yu, and Meng Yang. Large-margin softmax loss for convolutional neural networks. In *ICML*, 2016. 2

- [36] Ziwei Liu, Raymond A Yeh, Xiaoou Tang, Yiming Liu, and Aseem Agarwala. Video frame synthesis using deep voxel flow. In *ICCV*, pages 4463–4471, 2017. 1
- [37] Ilya Loshchilov and Frank Hutter. Sgdr: Stochastic gradient descent with warm restarts. *arXiv preprint arXiv:1608.03983*, 2016. 11
- [38] Laurens van der Maaten and Geoffrey Hinton. Visualizing data using t-sne. *Journal of machine learning research*, 9:2579–2605, 2008. 8
- [39] Ishan Misra and Laurens van der Maaten. Self-supervised learning of pretext-invariant representations. In *CVPR*, pages 6707–6717, 2020. 1, 2, 5, 6, 7, 11
- [40] Takeru Miyato, Shin-ichi Maeda, Masanori Koyama, and Shin Ishii. Virtual adversarial training: a regularization method for supervised and semi-supervised learning. *TPAMI*, 41(8):1979–1993, 2018. 7
- [41] Mehdi Noroozi and Paolo Favaro. Unsupervised learning of visual representations by solving jigsaw puzzles. In *ECCV*, 2016. 1
- [42] Aaron van den Oord, Yazhe Li, and Oriol Vinyals. Representation learning with contrastive predictive coding. *arXiv preprint arXiv:1807.03748*, 2018. 1, 2, 3, 6
- [43] Deepak Pathak, Philipp Krahenbuhl, Jeff Donahue, Trevor Darrell, and Alexei A Efros. Context encoders: Feature learning by inpainting. In *CVPR*, 2016. 1
- [44] Shaoqing Ren, Kaiming He, Ross Girshick, and Jian Sun. Faster r-cnn: Towards real-time object detection with region proposal networks. In *NeurIPS*, pages 91–99, 2015. 6
- [45] Yonglong Tian, Dilip Krishnan, and Phillip Isola. Contrastive multiview coding. *arXiv preprint arXiv:1906.05849*, 2019. 1, 2, 6
- [46] Feng Wang, Jian Cheng, Weiyang Liu, and Haijun Liu. Additive margin softmax for face verification. *IEEE Signal Processing Letters*, 2018. 2
- [47] Hao Wang, Yitong Wang, Zheng Zhou, Xing Ji, Dihong Gong, Jingchao Zhou, Zhifeng Li, and Wei Liu. Cosface: Large margin cosine loss for deep face recognition. In *CVPR*, pages 5265–5274, 2018. 2
- [48] Yuxin Wu, Alexander Kirillov, Francisco Massa, Wan-Yen Lo, and Ross Girshick. Detectron2, 2019. 6
- [49] Zhirong Wu, Yuanjun Xiong, Stella X Yu, and Dahua Lin. Unsupervised feature learning via non-parametric instance discrimination. In *CVPR*, pages 3733–3742, 2018. 1, 2, 3, 5, 6, 7, 8, 11
- [50] Junyuan Xie, Ross Girshick, and Ali Farhadi. Unsupervised deep embedding for clustering analysis. In *ICML*, 2016. 1, 2
- [51] Jianwei Yang, Devi Parikh, and Dhruv Batra. Joint unsupervised learning of deep representations and image clusters. In *CVPR*, 2016. 1, 2
- [52] Mang Ye, Xu Zhang, Pong C Yuen, and Shih-Fu Chang. Unsupervised embedding learning via invariant and spreading instance feature. In *CVPR*, pages 6210–6219, 2019. 1, 2
- [53] Xiaohua Zhai, Avital Oliver, Alexander Kolesnikov, and Lucas Beyer. S4l: Self-supervised semi-supervised learning. In *ICCV*, pages 1476–1485, 2019. 7
- [54] Xiaohang Zhan, Xingang Pan, Ziwei Liu, Dahua Lin, and Chen Change Loy. Self-supervised learning via conditional motion propagation. In *CVPR*, 2019. 1
- [55] Xiaohang Zhan, Jiahao Xie, Ziwei Liu, Yew-Soon Ong, and Chen Change Loy. Online deep clustering for unsupervised representation learning. In *CVPR*, pages 6688–6697, 2020. 1, 2, 6
- [56] Liheng Zhang, Guo-Jun Qi, Liqiang Wang, and Jiebo Luo. Aet vs. aed: Unsupervised representation learning by auto-encoding transformations rather than data. In *CVPR*, pages 2547–2555, 2019. 1
- [57] Richard Zhang, Phillip Isola, and Alexei A Efros. Colorful image colorization. In *ECCV*, 2016. 1
- [58] Richard Zhang, Phillip Isola, and Alexei A Efros. Split-brain autoencoders: Unsupervised learning by cross-channel prediction. In *CVPR*, 2017. 5
- [59] Bolei Zhou, Agata Lapedriza, Jianxiong Xiao, Antonio Torralba, and Aude Oliva. Learning deep features for scene recognition using places database. In *NeurIPS*, pages 487–495, 2014. 5
- [60] Chengxu Zhuang, Alex Lin Zhai, and Daniel Yamins. Local aggregation for unsupervised learning of visual embeddings. In *ICCV*, pages 6002–6012, 2019. 1, 2, 6

## Appendix

In this appendix, we first provide the implementation details for pre-training and transfer learning in Section A and Section B, respectively. We then provide the per-shot results for the low-shot VOC07 classification benchmark in Section C. Finally, we further analyze the benefits of inter-image invariance brought by InterCLR through KNN visualization in Section D.

### A. Unsupervised pre-training details

To ensure fair comparisons, we follow the same settings of the base methods for unsupervised pre-training.

**NPIDv2-InterCLR.** Our improved version of NPID [49] (*i.e.*, NPIDv2) extends the original data augmentation in [49] by including Gaussian blur in [8]. However, we do not use the same heavy color distortion as [8] since it has diminishing gains in our higher baseline. Instead, we only apply a color jittering with a saturation factor in  $[0, 2]$ , and a hue factor in  $[-0.5, 0.5]$ . We also add a 2-layer MLP projection head (with a 2,048-dimensional hidden layer and ReLU) to project high-dimensional features into a 128-D L2-normalized embedding space following [8]. We use SGD as the optimizer with a momentum of 0.9 and a weight decay of  $10^{-4}$ . We adopt the cosine learning rate decay schedule [37] with an initial learning rate of 0.03 using a batch size of 256 for 200 epochs. We set the temperature parameter  $\tau = 0.1$ , the number of negative samples  $K = 16, 384$ , and the momentum coefficient  $\omega = 0.5$ .

The aforementioned modifications make NPIDv2 a stronger baseline, upon which we build InterCLR. Yet, NPIDv2-InterCLR substantially outperforms NPIDv2 as shown in the main paper. For inter-image branch, we use online pseudo-label maintenance, semi-hard negative sampling, and cosine margin  $m = -0.5$  for  $\mathcal{L}_{\text{Inter-MarginNCE}}$ . We do not use any cosine margin for intra-image branch to solely verify the effectiveness of inter-image branch. We find over-clustering to be beneficial and set the number of clusters as 10,000, which is 10 times of the annotated number of ImageNet classes. We set the final loss weight  $\lambda = 0.75$  in Equation (6) of the main paper.

**MoCov2-InterCLR.** We maintain an additional memory bank to store all features from the momentum-updated encoder of MoCov2 for online clustering. We set the number of negative samples  $K = 16, 384$ , and the momentum coefficient  $\omega = 1$  for the memory bank. We use online pseudo-label maintenance, semi-hard negative sampling, and cosine margin  $m = -0.5$  only for  $\mathcal{L}_{\text{Inter-MarginNCE}}$ . We set the number of clusters as 10,000 and the final loss weight  $\lambda = 0.75$ . Other hyper-parameters including MLP projection head, temperature parameter, training procedure and data augmentation setting exactly follow [9].

**BYOL-InterCLR.** We exactly follow [22] for the training

hyper-parameters and augmentation recipes. Considering that many previous methods report their performance on 200 epochs, we also train for 200 epochs for fair comparisons, following the 300-epoch recipes in [22]: base learning rate is 0.3, weight decay is  $10^{-6}$ , and the base target exponential moving average parameter is 0.99. The same 200-epoch recipes are also adopted in [10]. Similar to MoCov2-InterCLR, we use a memory bank to store all features from the target network of BYOL to facilitate online clustering. Since BYOL uses a mean squared error loss without negative samples, we do not use any negative sampling and cosine margin in this entry. Instead, we only sample the positive pair after clustering and adopt the same loss in place of the MarginNCE loss for inter-image invariance learning. Following NPIDv2 and MoCov2 experiments, we set the number of clusters as 10,000 and the final loss weight  $\lambda = 0.75$ . Although no negative pairs are sampled for inter-image branch, we empirically observe no collapsing solutions due to the stop-gradient operation introduced in BYOL.

### B. Transfer learning details

**Image classification with linear models.** For ImageNet and Places205, we train linear models on the frozen representations using SGD with a momentum of 0.9. For ImageNet, we train for 100 epochs, with a batch size of 256 and a weight decay of  $10^{-4}$ . The learning rate is initialized as 0.01, decayed by a factor of 10 after every 30 epochs. For Places205, we train for 28 epochs, with a batch size of 256 and a weight decay of  $10^{-4}$ . The learning rate is initialized as 0.01, dropped by a factor of 10 at three equally spaced intervals. Other hyper-parameters are set following [20]. We report top-1 center-crop accuracy on the official validation split of ImageNet and Places205. For VOC07, we use the conv5 features (average pooled to around 9,000 dimensions) of ResNet-50. We follow the same setup in [20, 39] and train linear SVMs on the frozen representations using LIBLINEAR package [18]. We train on the trainval split of VOC07 and report mAP on the test split.

**Low-shot image classification.** We use the conv5 features (average pooled to around 9,000 dimensions) of ResNet-50 and train linear SVMs on the frozen representations following the same procedure in [20]. We train on the trainval split of VOC07 and report mAP on the test split.

**Semi-supervised learning.** We fine-tune ResNet-50 models using SGD with a momentum of 0.9 and a batch size of 256. We use the 1% and 10% ImageNet subsets specified in the official code release of SimCLR [8]. For both 1% and 10% labeled data, we fine-tune for 20 epochs, with the initial learning rate of backbone set as 0.01 and that of linear classifier as 1. The learning rate is decayed by a factor of 5 at 12 and 16 epochs. We use a weight decay of  $5 \times 10^{-4}$  for 1% fine-tuning and  $10^{-4}$  for 10% fine-tuning.

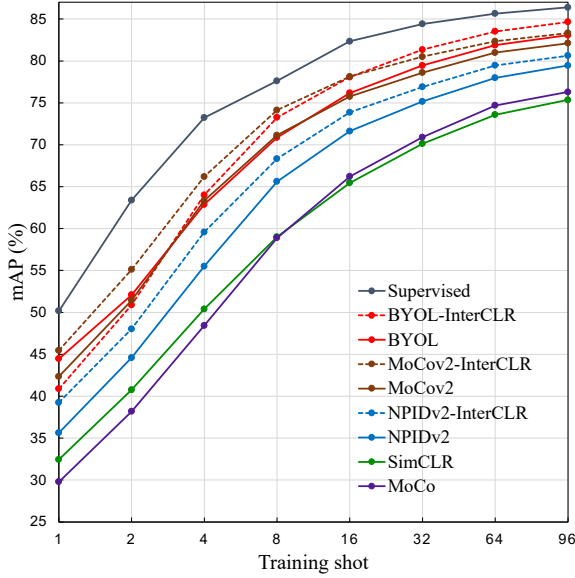


Figure 9. Low-shot image classification on VOC07 with linear SVMs trained on the features from the best-performing layer of each method for ResNet-50. All methods are pre-trained for 200 epochs on ImageNet for fair comparisons. We show the average performance for each shot across five runs.

**Object detection.** We follow the evaluation protocol from MoCo [23] for object detection. Specifically, we use a batch size of 2 images per GPU, a total of 8 GPUs and fine-tune ResNet-50 models for 24k iterations ( $\sim 23$  epochs). The learning rate is initialized as 0.02 with a linear warmup for 100 iterations, and decayed by a factor of 10 at 18k and 22k iterations. The image scale is  $[480, 800]$  pixels during training and 800 at inference. Following [10], we also search the fine-tuning learning rate for BYOL experiments.

### C. Per-shot results for low-shot classification

In Figure 9, we provide the per-shot results for the low-shot VOC07 classification benchmark. The final averaged mAP results of all low-shot values and all independent runs have been shown in Table 1 of the main paper. InterCLR improves upon all baselines and gradually bridges the gap to supervised pre-training when the number of labeled examples per class is increasing.

### D. KNN visualization

In Figure 10, we visualize some top-10 nearest neighbors retrieved with cosine similarity in the embedding space using the features learned by InterCLR. Compared with its intra-image invariance learning baseline, *i.e.*, Baseline (Intra), InterCLR (Intra+Inter) retrieves more correct images. Besides, InterCLR (Intra+Inter) also achieves higher cosine similarity with the queries than its intra-image invariance

counterpart. We observe this not only for the same correctly retrieved samples, but also for the whole 10 retrieved nearest neighbors: even the 10th nearest neighbor retrieved by InterCLR (Intra+Inter) obtains higher cosine similarity than the 1st nearest neighbor retrieved by the baseline.

The aforementioned gap is due to the inherent limitation of intra-image invariance learning: *only encouraging the similarity of different augmented views of the same image while discouraging the similarity of different images even though they should belong to the same semantic class*. This further demonstrates the benefits of inter-image invariance brought by InterCLR.

























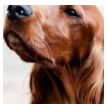










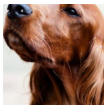

































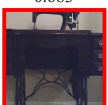
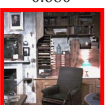
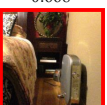
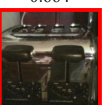
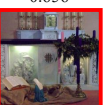
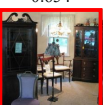
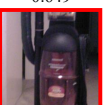











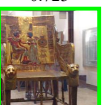


Query		Retrievals									
Baseline (Intra)		0.822	0.816	0.786	0.779	0.773	0.770	0.768	0.761	0.760	0.747
											
InterCLR (Intra+Inter)		0.902	0.868	0.856	0.855	0.851	0.849	0.849	0.840	0.834	0.834
											
Baseline (Intra)		0.834	0.827	0.819	0.800	0.793	0.786	0.783	0.772	0.769	0.763
											
InterCLR (Intra+Inter)		0.904	0.894	0.891	0.887	0.882	0.859	0.850	0.841	0.839	0.835
											
Baseline (Intra)		0.699	0.697	0.688	0.680	0.676	0.676	0.672	0.663	0.658	0.657
											
InterCLR (Intra+Inter)		0.789	0.775	0.773	0.770	0.765	0.755	0.753	0.752	0.752	0.750
											
Baseline (Intra)		0.683	0.680	0.668	0.664	0.656	0.654	0.649	0.645	0.645	0.644
											
InterCLR (Intra+Inter)		0.768	0.762	0.758	0.757	0.727	0.727	0.725	0.723	0.722	0.715
											

Figure 10. Retrieval results of some example queries on ImageNet. We compare InterCLR with its intra-image invariance learning baseline, *i.e.*, Baseline (Intra). The left-most column are queries from the validation set, while the right columns show 10 nearest neighbors retrieved from the training set with the similarity measured by cosine similarity. The positive retrieved results are framed in **green**, while the negative retrieved results are framed in **red**. Number on the top of each retrieved sample denotes the cosine similarity with its corresponding query.